Quantum Tunneling of Water in Beryl: A New State of the Water Molecule

Alexander I. Kolesnikov,[1,*] George F. Reiter,[2] Narayani Choudhury,[3] Timothy R. Prisk,[4] Eugene Mamontov,[1] Andrey Podlesnyak,[5] George Ehlers,[5] Andrew G. Seel,[6,†] David J. Wesolowski,[4] and Lawrence M. Anovitz[4]
[1]*Chemical and Engineering Materials Division, Oak Ridge National Laboratory, Oak Ridge, Tennessee 37831, USA*
[2]*Physics Department, University of Houston, Houston, Texas 77204, USA*
[3]*Math and Science Division, Lake Washington Institute of Technology, Kirkland, Washington 98034, USA; School of Science, Technology, Engineering and Math, University of Washington, Bothell, Washington 98011, USA*
[4]*Chemical Sciences Division, Oak Ridge National Laboratory, Oak Ridge, Tennessee 37831, USA*
[5]*Quantum Condensed Matter Division, Oak Ridge National Laboratory, Oak Ridge, Tennessee 37831, USA*
[6]*ISIS Facility, Rutherford Appleton Laboratory, Chilton, Didcot OX11 0QX, United Kingdom*
(Received 18 November 2015; published 22 April 2016)

Using neutron scattering and *ab initio* simulations, we document the discovery of a new "quantum tunneling state" of the water molecule confined in 5 Å channels in the mineral beryl, characterized by extended proton and electron delocalization. We observed a number of peaks in the inelastic neutron scattering spectra that were uniquely assigned to water quantum tunneling. In addition, the water proton momentum distribution was measured with deep inelastic neutron scattering, which directly revealed coherent delocalization of the protons in the ground state.

DOI: 10.1103/PhysRevLett.116.167802

Water is an essential material on Earth, exhibiting a number of anomalous physical properties in bulk states and under confinement [1–10]. Confined water can be almost free [11], without hydrogen bonds (HB) and display significant quantum behavior. Inelastic neutron scattering (INS) studies have demonstrated that in fullerenes such water exhibits quantum transitions between the para and ortho states [12,13], and it has been suggested that quantum tunneling of water explains the fine structure of the optical spectra of beryl [14,15]. INS provides a unique method to study the vibrational and quantum tunneling dynamics of hydrogen-containing materials because of the anomalously large incoherent neutron scattering cross section of protium (H-1). However, while INS studies have demonstrated hydrogen quantum tunneling in a number of systems, such as atomic hydrogen in metals [16], and rotational tunneling of methyl and ammonia groups [17], such behavior has not yet been demonstrated for water. Our recent INS studies of beryl using high incident neutron energies [18,19] have shown that the effective potential for water across the channel is very shallow. The corresponding INS spectrum is similar to the neutron recoil scattering of free protons, and energies of the observed intramolecular bending and stretching modes of water (197.5 and 465 meV, respectively) are consistent with a lack of hydrogen bonding.

This study considered the dynamics of water in low-alkali beryl single crystals (~0.1 wt % of Na, see Supplemental Material [20]). The structure of beryl ($Be_3Al_2Si_6O_{18}$, space group $P6/mcc$) contains six-membered rings of SiO_4 tetrahedra with open channels along the c axis [21] [Fig. 1(c)]. The channels form narrow (~2.8 Å) "bottlenecks" separating larger cavities 5.1 Å in diameter, which may contain alkali cations and water. Taking into account that the absence of the hydrogen bonding requires the water proton to cage-oxygen distance to be greater than 2.3 Å, the beryl cavity size is large enough to accommodate one nonhydrogen bonded water molecule, with no more free space available. In alkali-poor beryl, the water dipole moment is in the ab plane perpendicular to the channels, and water protons are distributed in 6×2 equivalent positions across the channel, above and below the oxygen site.

Figures 1(a) and 1(b) show the dynamical structure factor $S(\mathbf{Q}, E)$ of water in beryl for two orientations, $\mathbf{Q} \| c$ axis and $\mathbf{Q} \perp c$ axis, measured with incident neutron energies of $E_i = 25$ meV at the SEQUOIA and $E_i = 3$ meV at the CNCS spectrometers at the Spallation Neutron Source, Oak Ridge National Laboratory. The INS spectra exhibit three isotropic peaks at energies $E = 0.66$, 1.49, and 1.63 meV, four peaks at 0.27, 8.4, 12.7, and 14.7 meV for $\mathbf{Q} \perp c$ axis, and a peak at ~11 meV for $\mathbf{Q} \| c$ axis. Further measurements with higher energy resolution ($E_i = 10$ and 12 meV) showed that the peak at 8.4 meV is split into two with energies of 7.9 and 8.4 meV (see Supplemental Material Fig. S1 [20]).

The temperature dependence of the integrated intensities of these peaks clearly indicates their tunneling origin (with an exception of the peak at 11 meV, which is due to translational vibrations). Instead of growing with increasing temperature, as required for vibrational motions obeying Bose statistics, all peaks except that at 11 meV decrease in intensity in the neutron energy loss part of the spectra ($E > 0$ meV). This is characteristic of systems exhibiting quantum tunneling. The integrated intensities of the peaks with similar temperature dependencies $I(T)$ (except the peak at $E = 0.27$ meV) can be described by transitions of

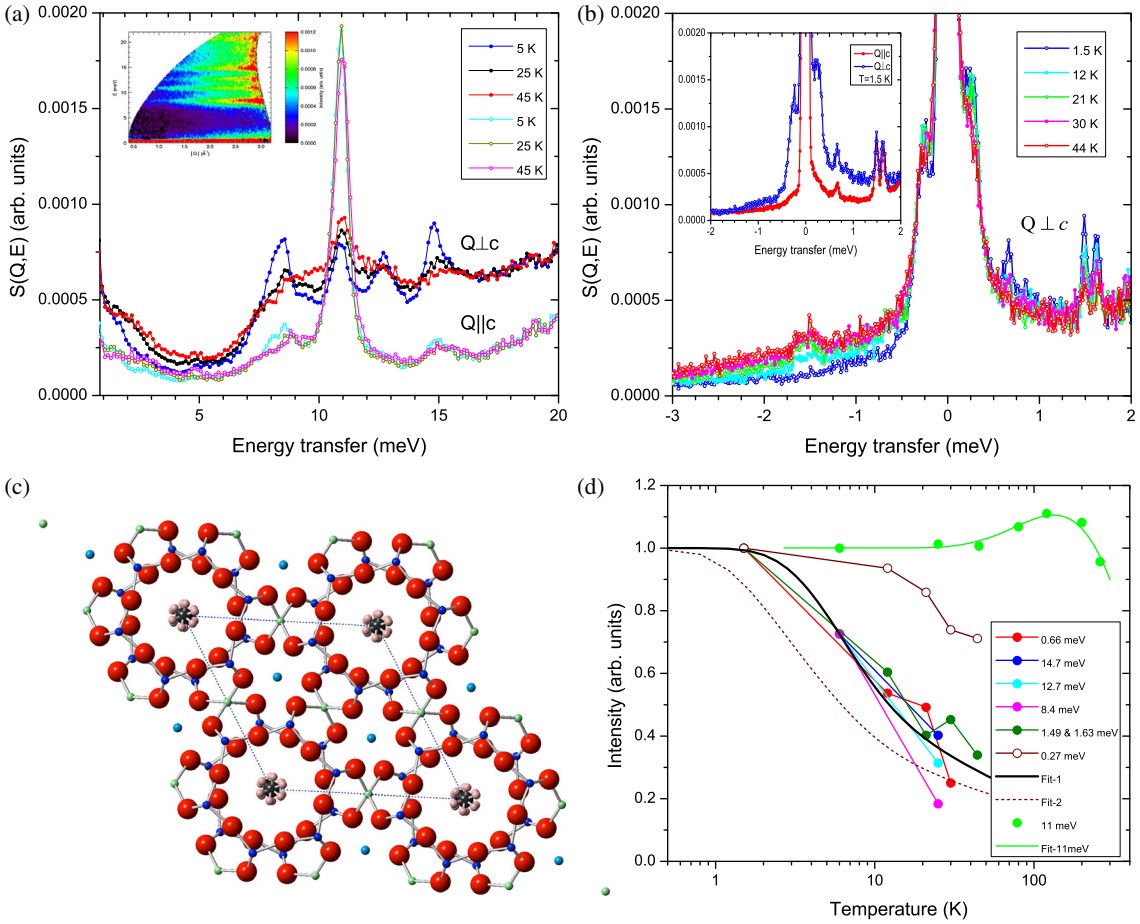

FIG. 1. INS spectra of water in beryl measured with (a) $E_i = 25$ meV and (b) and $E_i = 3$ meV. The inset in (a) shows contour plot of $S(\mathrm{Q}, E)$ at $T = 5$ K for $\mathbf{Q}\perp c$ axis. The enlarged version of this inset is presented in Supplemental Material Fig. S2 [20]. (c) Structure of beryl (view along the c axis), Si—blue, O—red, Al—blue grey, Be—green, H_2O—pink, and black (in the center of the channels). (d) Temperature dependence of the intensities of the tunneling peaks and the vibrational 11 meV peak in the INS spectra. The peaks' intensities are renormalized to be 1 at $T = 0$ K.

water protons from the lowest to higher split ground states [Fit 1 in Fig. 1(d)], which follow the expression:

$$I(T) \propto 1/\left[1 + \sum_{i=1}^{N} \exp\left(-\frac{E_i}{k_B T}\right)\right], \qquad (1)$$

where the E_i's are the energies of N split ground states relative to the lowest ground state. The peak at 0.27 meV has the same qualitative T and Q dependence as the other peaks, but its temperature dependence does not fall on the same trend as the other seven peaks, and its origin is unknown. The use of all eight peaks in the Eq. (1), however, fails to describe the experimental data [Fit 2 in Fig. 1(d)].

By contrast, the strong peak at 11 meV can be assigned to translational vibrations of water along the c axis (the librational modes should be more intense for $\mathbf{Q}\perp c$ axis). The intensity of the 11 meV peak first increases as the temperature is raised to 130 K, obeying the Bose population factor $n_B(E, T) = 1/[\exp(E/k_B T) - 1]$, then decreases due to the Debye-Waller factor. This dependence can be described [Fig. 1(d)] as $I(T) \propto \exp[-(\mathbf{Q}\mathbf{u}_\mathrm{H})^2][n_B(E, T) + 1]$, where $\mathbf{u}_\mathrm{H}$ is a vector of water proton displacement due to all vibrational modes.

For a particle jumping over six positions on a circle of radius d, the inelastic incoherent structure factor (IISF) can be expressed as [22]

$$\mathrm{IISF}(Q) \propto \frac{1}{6\pi} \sum_{l=1}^{5} \sum_{k=1}^{6} j_0\left(2Qd \sin\frac{\pi k}{6}\right) \cos\left(\frac{2\pi l k}{6}\right). \qquad (2)$$

This function is illustrated in the Supplemental Material Fig. S3 [20]. It strongly increases in the range of Q probed in these INS studies ($Q < 4$ Å^{-1}), as was observed in our experiments [see inset in Fig. 1(a), and Supplemental Material Figs. S2 and S3 [20]]. While the observed temperature dependences could be due to magnetic impurities in the beryl and corresponding splitting of the ground state due to crystal field effects, the intensities of such peaks would have to obey the magnetic form factor of the impurity atoms, implying that the peak intensities must

decrease with increasing Q. No such behavior is observed in our data.

The seven peaks observed in the INS spectra, therefore, have both the characteristic temperature and momentum transfer dependence of quantum tunneling, and can be assigned to transitions from lower to higher levels of the ground state of water protons, which is split due to water tunneling between the sixfold equivalent positions within the beryl channel. While optical spectroscopic studies of synthetic beryl recently also proposed [14,15,23] that the water undergoes quantum tunneling, these data were subjected to complex treatment to extract energies and intensities of the excitations, and the reported transitions at 1.33 and 3.21 meV are inconsistent with the INS data, which are *sensitive primarily to the motion of individual hydrogen atoms.*

INS spectra of water in beryl do not show transitions between the para- and ortho-spin isomer forms of water, which were observed in $H_2O@C_{60}$ endofullerene [12,13], where water also demonstrates absence of HB and rotates almost freely, but did not exhibit evidence of tunneling. The absence of the transitions between the para and ortho states in the INS spectra of beryl is probably linked to the fact that water is not as free as in the case of fullerenes (it has a dipole moment perpendicular to the c axis and it occupies sixfold equivalent positions across the channel).

Further evidence for rotational tunneling of the water in beryl has been obtained from deep inelastic neutron scattering (DINS) measurements of the momentum distribution $n(\mathbf{p})$ of the water protons, collected at the VESUVIO spectrometer, ISIS neutron facility, Rutherford Appleton Laboratory. DINS is INS in the limit of large momentum transfer Q ($30 - 100$ Å^{-1}), when the neutrons scatter from individual atoms like freely moving particles scatter from each other [24]. Thus, the DINS spectrum depends only on the momentum distribution, or probability, $n(\mathbf{p})$, that the atom (of mass M) had a particular momentum ($\mathbf{p}$) at the time it was struck by the neutron

$$S(\mathbf{Q},E) = \int n(\mathbf{p})\delta\left[E - \frac{(\mathbf{p}+\hbar\mathbf{Q})^2}{2M} + \frac{p^2}{2M}\right] d\mathbf{p}. \quad (3)$$

At the temperature of the measurement, $T = 4.3$ K, the protons are substantially in the ground state of the system. If the water molecules undergo rotational tunneling, then $n(\mathbf{p})$ will include oscillations or interference fringes as a function of angle. On the other hand, if the water molecules are statically disordered within the pore channels, then $n(\mathbf{p})$ will be an ensemble average over molecules occupying the six possible positions, and no interference fringes will be observed.

DINS measurements were done for two orientations of the beryl crystal: with the c axis parallel and perpendicular (vertical) to the incoming neutron beam. Both configurations were fitted simultaneously to a single momentum distribution that is the average distribution of the two protons of the water molecule. The fitting procedure makes use of a basis of Hermite polynomials and spherical harmonics [25]. All

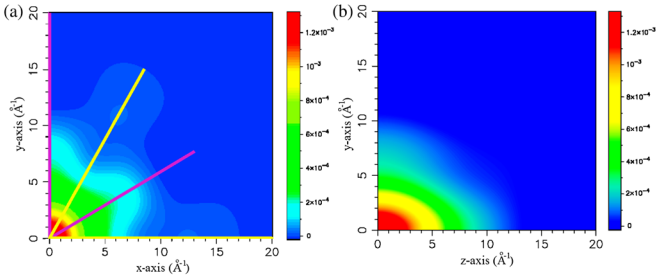

FIG. 2. Projection of water proton momentum distribution $n(\mathbf{p})$ in beryl onto the xy and yz planes (a) and (b), respectively, obtained from the DINS data. The second maximum in the radial direction [along yellow line in (a)] indicates that the proton is coherently delocalized in the channel, as a consequence of its ground state being coherently distributed (tunneling) between the six minima of the beryl potential.

terms consistent with the sixfold symmetry of the channel up to the eighth order Hermite polynomial were kept. In the fitting, we took the z axis to be along the crystal c axis, and the xy plane to be perpendicular to z (or parallel to the ab plane). Figure 2 shows contour plots of $n(\mathbf{p})$ in the xy and zy planes. The variation of the momentum width with angle [pink and yellow lines in panel (a)] is a result of the compression and elongation of the covalent bond of the water in the potential of the beryl cage as the molecule rotates. The appearance of the second maximum in the radial direction, dependent on angle (yellow line) shows that the proton is coherently distributed in the channel, as a consequence of its tunneling between the six minima of the beryl cage.

The anisotropy of the binding potential of the water protons is also reflected in $n(\mathbf{p})$. The statistical variances of $n(\mathbf{p})$, $\sigma_x = 3.66$ Å^{-1}, $\sigma_y = 3.61$ Å^{-1}, and $\sigma_z = 4.98$ Å^{-1} show that $n(\mathbf{p})$ is 37% broader in the direction parallel to the c axis than in the ab plane, indicating large proton delocalization across the channels, consistent with our INS data [18,19]. The average kinetic energy E_k is proportional to the second moment of $n(\mathbf{p})$ as:

$$E_k = \frac{\hbar^2}{2M}(\sigma_x^2 + \sigma_y^2 + \sigma_z^2), \quad (4)$$

yielding 106 meV for water protons, which is much smaller than in bulk water (~150 meV). A similar depression of the average kinetic energy ($E_k = 104$ meV) has been observed for water confined within single-walled carbon nanotubes [25]. To underscore this point, one may estimate the E_k of water protons by assuming that it is given by the zero-point energies of the intramolecular bending and stretching modes taken as simple harmonic oscillators [26]. Because the energy of the stretching modes of water in beryl (465 meV) is much larger than in bulk water or ice and the energy of the bending modes changes only a little, the use of only intramolecular modes gives $E_k = 132.5$ meV, which is significantly larger than the experimental value 106 meV and indicates strong delocalization of the proton in the tunneling state of water in beryl. The coherent compression

and elongation of the covalent bond of the water molecule leads to a broad spatial distribution of the protons in the radial direction in the ground state. The concomitant narrowing of the momentum distribution is reflected in the reduction in the measured kinetic energy. At the same time, the potential surface related to the covalent bond is nearly harmonic on the energy scale above the ground state. We see, therefore, in the vibrational spectrum, that the stretch mode occurs at the frequency of the free molecule, despite the overall reduction of the kinetic energy in the ground state. The anharmonicity induced in the potential by the interaction with the beryl cage has the effect of changing the excitation energy with the displacement of the oscillator and leads to an additional broadening of the stretching mode, as observed.

To further elucidate the neutron scattering results on the dynamics of water in beryl, a combination of *ab initio* density functional theory (DFT) calculations and path integral molecular dynamics (PIMD) simulations was employed (see Supplemental Material [20]). DFT calculations for sodium-free beryl with water were carried out using the code ABINIT [27]. The computed structure of beryl (see Supplemental Material Fig. S4 [20]) was found to be in excellent agreement with experiment [21]. The calculated O-H bond distance is 0.949 Å and the H-O-H bond angle is 106.9°, the hydrogen atoms are distributed in six equivalent positions, and the average H-H vector is oriented around 3.97° relative to c axis. *Ab initio* studies reveal that the water oxygen is also dynamically disordered and can be positioned in multiple sites, giving rise to multiple ground states. Typical water oxygen in-plane distortions of fractional coordinates are about (0, 0.022, 0.25), i.e., ∼0.2 Å from the center of the channel.

DFT calculations show that in the equilibrium (static) state neglecting quantum fluctuations, the potential barrier for water rotation around the c axis is rather large (about 176 meV, see Supplemental Material Fig. S5 [20]). Vibrations of the beryl cage, however, allow adiabatic coincidence states for some phonon modes in the vicinity of zone center and a zone boundary, where the barriers are significantly lowered (down to 48–56 meV). The eigenvectors of these phonon modes typically involve beryl framework rotations. A zone center configuration with minimum energy for rotation was used as a starting adiabatic "coincidence" configuration for PIMD simulations [28–31]. The calculated charge density of water shows delocalization of protons [Fig. 3(a)] over a hexagonal ring that spatially extends to a width of around 1.2 Å, which is evidence of water tunneling (phonon assisted tunneling). The oxygen map also reveals reasonably large distribution of the oxygen atom. Similar broadening of the electronic density of states due to proton delocalization in bulk liquid water has also been reported in Ref. [31].

The rotational energies and tunneling splittings are calculated from an effective one dimensional adiabatic potential with sixfold symmetry for rotation of water molecule around

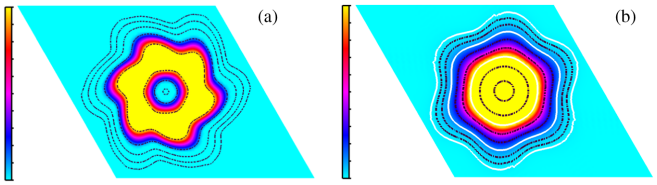

FIG. 3. The calculated charge density slices in the ab plane giving the proton map (a) and oxygen map (b), respectively, for the water molecule confined in beryl. The charge densities are obtained from the computed DFT/PIMD structures. The contours represent isoenergy lines; the bounding box is (−0.18, 0.18) along the a and b axes. The min or max charge (absolute values) in the color bars are 0.0224/0.0985 Ha/Å^3 and 0.0224/13.6546 Ha/Å^3 in (a) and (b), respectively.

the c axis (see Supplemental Material Table SI [20]). The calculated tunneling peaks are at about 2.7, 10.1, and 16.7 meV and the first two peaks are double degenerate. Delocalization yields distortions from sixfold symmetry, which can be seen as the skewing and asymmetry in the calculated proton density [Fig. 3(a)]. Interestingly, the difference-Fourier map of the proton density obtained in a neutron diffraction experiment (see Fig. 2 in Ref. [21]) also reveals some asymmetry. Symmetry lowering distortions remove the degeneracies in the energy levels, in agreement with split tunneling peaks at 1.49 and 1.63 meV, and 7.9 and 8.4 meV observed in INS data, and could also result in appearing of additional tunneling peaks. The averaged expected error of our calculated ground state levels due to alteration of the moment of inertia and barrier height values was estimated using computed lower and upper bounds for barrier heights and moment of inertia, and is about ±1.4 meV. Therefore, the calculated tunneling peaks with an expected spread of about ±1.4 meV are in reasonable agreement with INS data.

The present work has shown, using neutron scattering methods and *ab initio* simulations, that water in the channels in the beryl structure tunnels between the six symmetrically equivalent positions around the c axis. This presents a new state of the water molecule, having an anomalously small proton kinetic energy due to spatial delocalization. The observed tunneling state of water in beryl is rather unusual, compared to other known examples of rotational tunneling of molecules, e.g., methyl and ammonia groups [17], where the tunneling and localized (nontunneling) molecules look unchanged (except for overlapping of the corresponding proton wave functions in the tunneling state, there is no difference between these molecules, because all constitute protons occupy the same positions). In the case of water in beryl, however, water protons in the tunneling state occupy different positions compared to the nontunneling molecule: the center of gravity of the water molecule and its dipole moment are, therefore, modified by the tunneling. Due to the observation of multiple tunneling peaks in the INS spectra and the coherent delocalization of protons identified from the DINS data, we consider that tunneling water can be described

as water with delocalized protons over all possible positions across the beryl channel, and therefore can be called "a new state of the water molecule".

This material is primarily based upon work supported by the U.S. Department of Energy, Office of Science, Office of Basic Energy Sciences, Chemical Sciences, Geosciences, and Biosciences Division. The neutron scattering experiments at Oak Ridge National Laboratory's Spallation Neutron Source were sponsored by the Scientific User Facilities Division, Office of Basic Energy Sciences, U.S. Department of Energy. The STFC Rutherford Appleton Laboratory is thanked for access to neutron beam facilities. Some of the beryl crystals used in our experiments were cut by Bradley S. Wilson of Coast-to-Coast Rarestones, International. N. C. also gratefully acknowledges research support from the University of Washington (DOE/UW Grants No. 4000127504, No. 6400012674; No. 66-1283).

This manuscript has been authored by UT-Battelle, LLC under Contract No. DE-AC05-00OR22725 with the U.S. Department of Energy. The United States Government retains and the publisher, by accepting the article for publication, acknowledges that the United States Government retains a nonexclusive, paid-up, irrevocable, world-wide license to publish or reproduce the published form of this manuscript, or allow others to do so, for United States Government purposes. The Department of Energy will provide public access to these results of federally sponsored research in accordance with the DOE Public Access Plan.

*kolesnikovai@ornl.gov

†Present address: Inorganic Chemistry Department, University of Oxford, South Parks Road, Oxford OX1 3QR, United Kingdom.

[1] P. Ball, Water—An enduring mystery, Nature (London) **452**, 291 (2008).

[2] J. L. Finney, Water? What's so special about it?, Phil. Trans. R. Soc. B **359**, 1145 (2004).

[3] C. A. Angell, Insights into phases of liquid water from study of its unusual glass-forming properties, Science **319**, 582 (2008).

[4] P. G. Debenedetti and H. E. Stanley, Supercooled and glassy water, Phys. Today **56**, 40 (2003).

[5] J. Israelachvili and H. Wennerström, Role of hydration and water structure in biological and colloidal interactions, Nature (London) **379**, 219 (1996).

[6] G. Algara-Siller, O. Lehtinen, F. C. Wang, R. R. Nair, U. Kaiser, H. A. Wu, A. K. Geim, and I. V. Grigorieva, Square ice in graphene nanocapillaries, Nature (London) **519**, 443 (2015).

[7] K. Koga, G. T. Gao, H. Tanaka, and X. C. Zeng, Formation of ordered ice nanotubes inside carbon nanotubes, Nature (London) **412**, 802 (2001).

[8] A. I. Kolesnikov, J. M. Zanotti, C. K. Loong, P. Thiyagarajan, A. P. Moravsky, R. O. Loutfy, and C. J. Burnham, Anomalously Soft Dynamics of Water in a Nanotube: A Revelation of Nanoscale Confinement, Phys. Rev. Lett. **93**, 035503 (2004).

[9] H.-W. Wang, M. J. DelloStritto, N. Kumar, A. I. Kolesnikov, P. R. C. Kent, J. D. Kubicki, D. J. Wesolowski, and J. O. Sofo, Vibrational density of states of strongly H-bonded interfacial water: Insights from inelastic neutron scattering and theory, J. Phys. Chem. C **118**, 10805 (2014).

[10] G. F. Reiter, A. Deb, Y. Sakurai, M. Itou, V. G. Krishnan, and S. J. Paddison, Anomalous Ground State of the Electrons in Nanoconfined Water, Phys. Rev. Lett. **111**, 036803 (2013).

[11] K. Kurotobi and Y. Murata, A single molecule of water encapsulated in fullerene C_{60}, Science **333**, 613 (2011).

[12] C. Beduz *et al.*, Quantum rotation of ortho and para-water encapsulated in a fullerene cage, Proc. Natl. Acad. Sci. U.S.A. **109**, 12894 (2012).

[13] K. S. K. Goh *et al.*, Symmetry-breaking in the endofullerene $H_2O@C_{60}$ revealed in the quantum dynamics of ortho and para-water: A neutron scattering investigation, Phys. Chem. Chem. Phys. **16**, 21330 (2014).

[14] B. P. Gorshunov, E. S. Zhukova, V. I. Torgashev, V. V. Lebedev, G. S. Shakurov, R. K. Kremer, E. V. Pestrjakov, V. G. Thomas, D. A. Fursenko, and M. Dressel, Quantum behavior of water molecules confined to nanocavities in gemstones, J. Phys. Chem. Lett. **4**, 2015 (2013).

[15] B. P. Gorshunov *et al.*, THz-IR spectroscopy of single H_2O molecules confined in nanocage of beryl crystal lattice, Phase Transitions **87**, 966 (2014).

[16] H. Wipf, A. Magerl, S. M. Shapiro, S. K. Satija, and W. Thomlinson, Neutron-Spectroscopic Evidence for Hydrogen Tunneling States in Niobium, Phys. Rev. Lett. **46**, 947 (1981).

[17] M. Prager and A. Heidemann, Rotational tunneling and neutron spectroscopy: A compilation, Chem. Rev. **97**, 2933 (1997).

[18] L. M. Anovitz, E. Mamontov, P. ben Ishai, and A. I. Kolesnikov, Anisotropic dynamics of water ultraconfined in macroscopically oriented channels of single-crystal beryl: A multifrequency analysis, Phys. Rev. E **88**, 052306 (2013).

[19] A. I. Kolesnikov, L. M. Anovitz, E. Mamontov, A. Podlesnyak, and G. Ehlers, Strong anisotropic dynamics of ultra-confined water, J. Phys. Chem. B **118**, 13414 (2014).

[20] See the Supplemental Material at http://link.aps.org/supplemental/10.1103/PhysRevLett.116.167802, which includes Refs. [32–53], for details on the sample, the experimental methods, and *ab initio* calculations.

[21] G. Diego Gatta, F. Nestola, G. D. Bromiley, and S. Mattauch, The real topological configuration of the extra-framework content in alkali-poor beryl: A multi-methodological study, Am. Mineral. **91**, 29 (2006).

[22] J. D. Barnes, Inelastic neutron scattering study of the "rotator" phase transition in n-nonadecane, J. Chem. Phys. **58**, 5193 (1973).

[23] E. S. Zhukova *et al.*, Vibrational states of a water molecule in a nano-cavity of beryl crystal lattice, J. Chem. Phys. **140**, 224317 (2014).

[24] C. Andreani, D. Colognesi, J. Mayers, G. F. Reiter, and R. Senesi, Measurement of momentum distribution of light atoms and molecules in condensed matter systems using inelastic neutron scattering, Adv. Phys. **54**, 377 (2005).

[25] G. Reiter, C. Burnham, D. Homouz, P. M. Platzman, J. Mayers, T. Abdul-Redah, A. P. Moravsky, J. C. Li, C. K. Loong, and A. I. Kolesnikov, Anomalous Behavior of Proton

Zero Point Motion in Water Confined in Carbon Nanotubes, Phys. Rev. Lett. **97**, 247801 (2006).
[26] R. Moreh and D. Nemirovsky, On the proton kinetic energy in H_2O and in nanotube water, J. Chem. Phys. **133**, 084506 (2010).
[27] X. Gonze *et al.*, ABINIT: First-principles approach to material and nanosystem properties, Comput. Phys. Commun. **180**, 2582 (2009).
[28] G. Geneste, M. Torrent, F. Bottin, and P. Loubeyre, Strong Isotope Effect in Phase II of Dense Solid Hydrogen and Deuterium, Phys. Rev. Lett. **109**, 155303 (2012).
[29] G. Geneste, A. Ottochian, J. Hermet, and G. Dezanneau, Proton transport in barium stannate: classical, semi-classical and quantum regimes, Phys. Chem. Chem. Phys. **17**, 19104 (2015).
[30] M. Benoit, D. Marx, and M. Parrinello, Tunnelling and zero-point motion in high-pressure ice, Nature (London) **392**, 258 (1998).
[31] F. Giberti, A. A. Hassanali, M. Ceriotti, and M. Parrinello, The role of quantum effects on structural and electronic fluctuations in neat and charged water, J. Phys. Chem. B **118**, 13226 (2014).
[32] G. E. Granroth, A. I. Kolesnikov, T. E. Sherline, J. P. Clancy, K. A. Ross, J. P. C. Ruff, B. D. Gaulin, S. E. Nagler, SEQUOIA: A newly operating chopper spectrometer at the SNS, J. Phys. Conf. Ser. **251**, 012058 (2010).
[33] M. B. Stone *et al.*, A comparison of four direct geometry time-of-flight spectrometers at the Spallation Neutron Source, Rev. Sci. Instrum. **85**, 045113 (2014).
[34] G. Ehlers, A. A. Podlesnyak, J. L. Niedziela, E. B. Iverson, and P. E. Sokol, The new cold neutron chopper spectrometer at the Spallation Neutron Source: Design and performance, Rev. Sci. Instrum. **82**, 085108 (2011).
[35] O. Arnold *et al.*, Mantid-Data analysis and visualization package for neutron scattering and μSR experiments, Nucl. Instrum. Methods Phys. Res., Sect. A **764**, 156 (2014).
[36] R. T. Azuah, L. R. Kneller, Y. Qiu, P. L. W. Tregenna-Piggott, C. M. Brown, J. R. D. Copley, and R. M. Dimeo, DAVE: A comprehensive software suite for the reduction, visualization, and analysis of low energy neutron spectroscopic data, J. Res. Natl. Inst. Stand. Technol. **114**, 341 (2009).
[37] J. Mayers and M. A. Adams, Calibration of an electron volt neutron spectrometer, Nucl. Instrum. Methods Phys. Res., Sect. A **625**, 47 (2011).
[38] J. Mayers, A. Fielding, and R. Senesi, Multiple scattering in deep inelastic neutron scattering: Monte Carlo simulations and experiments at the ISIS eVS inverse geometry spectrometer, Nucl. Instrum. Methods Phys. Res., Sect. A **481**, 454 (2002).
[39] J. Mayers, Calculation of background effects on the VESUVIO eV neutron spectrometer, Meas. Sci. Technol. **22**, 015903 (2011).
[40] R. M. Martin, *Electronic Structure: Basic Theory and Practical Methods* (Cambridge University Press, Cambridge, UK, 2004).
[41] S. Baroni, S. de Gironcoli, A. D. Dal Corso, and P. Giannozzi, Phonons and related crystal properties from density-functional perturbation theory, Rev. Mod. Phys. **73**, 515 (2001).
[42] D. Marx and M. Parrinello, Ab initio path integral molecular dynamics: Basic ideas, J. Chem. Phys. **104**, 4077 (1996).
[43] D. Marx and M. Parrinello, Ab initio path-integral molecular dynamics, Z. Phys. B **95**, 143 (1994).
[44] X. Gonze *et al.*, First-principles computation of material properties: The ABINIT software project, Comput. Mater. Sci. **25**, 478 (2002).
[45] N. Choudhury, E. J. Walter, A. I. Kolesnikov, and C.-K. Loong, Large phonon band gap in $SrTiO_3$ and the vibrational signatures of ferroelectricity in $ATiO_3$ perovskites: First-principles lattice dynamics and inelastic neutron scattering, Phys. Rev. B **77**, 134111 (2008).
[46] K. Momma and F. J. Izumi, VESTA: A three-dimensional visualization system for electronic and structural analysis, J. Appl. Crystallogr. **41**, 653 (2008).
[47] M. Prencipe, Ab initio Hartree-Fock study and charge density analysis of beryl ($Al_4Be_6Si_{12}O_{36}$), Phys. Chem. Miner. **29**, 552 (2002).
[48] M. Prencipe, Y. Noel, B. Civalleri, C. Roetti, and R. Dovesi, Quantum-mechanical calculation of the vibrational spectrum of beryl ($Al_4Be_6Si_{12}O_{36}$) at the Γ point, Phys. Chem. Miner. **33**, 519 (2006).
[49] T. Pilati, F. Demartin, and C. M. Gramaciolli, Lattice-dynamical evaluation of thermodynamic properties and atomic displacement parameters for beryl using a transferable empirical force field, Am. Mineral. **82**, 1054 (1997).
[50] B. Charoy, P. de Donato, O. Barres, and C. Pinto-Coelho, Channel occupancy in an alkali-poor beryl from Serra Branca (Goias, Brazil): Spectroscopic characterization, Am. Mineral. **81**, 395 (1996).
[51] B. Winkler, The dynamics of H_2O in minerals, Phys. Chem. Miner. **23**, 310 (1996).
[52] R. M. Dimeo, Visualization and measurement of quantum rotational dynamics, Am. J. Phys. **71**, 885 (2003).
[53] J. Colmenero, A. J. Moreno, and A. Alegria, Neutron scattering investigations on methyl group dynamics in polymers, Prog. Polym. Sci. **30**, 1147 (2005).